ACS Photonics

Article

pubs.acs.org/journal/apchd5

Propagation of Channel Plasmons at the Visible Regime in Aluminum V-Groove Waveguides

Oren Lotan,[†] Cameron L. C. Smith,[‡] Jonathan Bar-David,[†] N. Asger Mortensen,[§] Anders Kristensen,[‡] and Uriel Levy*[,†]

[†]Department of Applied Physics, the Benin School of Engineering, the Center for Nanoscience and Nanotechnology, The Hebrew University of Jerusalem, Jerusalem, Israel

[‡]Department of Micro- and Nanotechnology, Technical University of Denmark, Kongens Lyngby DK-2800, Denmark

[§]Department of Photonics Engineering, Technical University of Denmark, Kongens Lyngby DK-2800, Denmark

Supporting Information

ABSTRACT: Aluminum plasmonics is emerging as a promising platform in particular for the ultraviolet-blue spectral band. We present the experimental results of propagating channel plasmon-polaritons (CPP) waves in aluminum coated V-shaped waveguides at the short visible wavelength regime. The V-grooves are fabricated by a process involving UV-photolithography, crystallographic silicon etching, and metal deposition. Polarization measurements of coupling demonstrate a preference to the TM-aligned mode, as predicted in simulations.

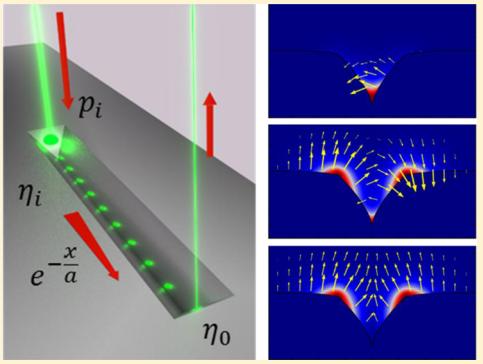

KEYWORDS: *plasmonic waveguides, aluminum plasmonics, V-groove waveguides*

Plasmonic waveguides are receiving growing attention in recent years.[1−7] Significant effort has been directed toward the infrared (IR) regime, motivated by the telecom applications around the wavelength of λ = 1550 nm. As a result, a major portion of the research was focused on waveguides consisting of gold (Au) or silver (Ag), which exhibit low losses in the IR regime. However, as the losses of these metals are very high in the short visible wavelengths primarily due to interband transitions,[8] the implementation of plasmonic waveguides at this spectral range is challenging. Considering the fact that plasmonic waveguides may have myriad possible applications at the visible range, from lab-on-chip biosensing devices[9] to nanoscopes,[10] obtaining high performance plasmonic waveguides in the short visible range, down to the ultraviolet (UV) is of a great need.

In an attempt to overcome the limitations of Au and Ag, it has been suggested that aluminum (Al) may be used as the material of choice for plasmonic devices in the visible and UV regimes, in which photon energies are higher than the Al interband transition energy, leading to a reduced absorption as compare with Au or Ag.[11−16] In this work we demonstrate experimentally the realization of aluminum plasmonic waveguides in a V-groove geometry, while our experiments are further supported by simulations. Previous studies have shown that V-groove plasmonic waveguides can be easily fabricated, allow efficient coupling even without the use of grating couplers,[17−19] can support highly confined CPP modes in the near IR when coated with Au, and offer a wide range of possibilities for plasmonic circuitry and manipulation of light in the nanoscale.[20−25] We show that V-groove plasmonic waveguides made of Al can support well-confined CPP modes at the short visible wavelength regime. The availability of such V groove based Al plasmonic waveguides enables interesting applications in areas such as quantum plasmonics, light harvesters, lab on chip components, as well as to the fundamental understanding of plasmon excitations and their interactions.[26]

Fabrication and Characterization. A scanning electron microscope (SEM) image of our waveguides is shown in Figure 1a,b. Each waveguide has a curved, V-shaped profile, a W = 3 μm width and length L ranging between 10 and 30 μm. Schematics of the device operation, including the coupling in and out, as well as the signal attenuation along the propagation direction, is illustrated in Figure 1c. Key steps in the fabrication process are illustrated in Figure 1d: UV photolithography followed by crystallographic etch in a KOH bath to define the V-groove and the termination mirrors (nanocouplers) simultaneously. A thermal oxidation is performed to modify the resulting V-groove profile to achieve more localized CPP modes. Finally, a thin layer of the desired metal (in our case Al) is evaporated on the surface (for further details, see ref 14).

Received: August 27, 2016
Published: October 10, 2016

DOI: 10.1021/acsphotonics.6b00648
ACS Photonics 2016, 3, 2150−2157

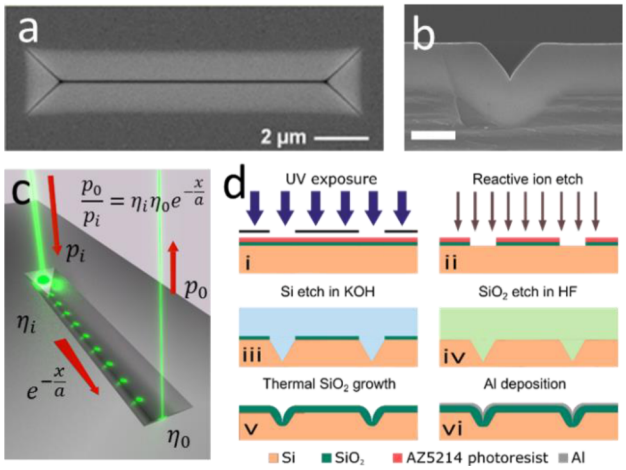

Figure 1. (a, b) Top view and cross section SEM image of the waveguide, respectively. Both scale bars are 2 μm; (c) Sketch of the coupling of light into the V-groove waveguide and the propagation of plasmons within it. Light from free space is coupled into SPPs and back into free space via a pair of tilted mirrors terminating the waveguide at both its ends and serving as nanocouplers; (d) Illustration of key steps in the fabrication of the V-groove waveguide.

Among other advantages, this process allows flexibility in the choice of metal, as the shape of the V-groove is imprinted on the Si-SiO layer, and therefore, the metal layer can be easily stripped away and be replaced by a different metal for another experiment, for example, a series of experiments utilizing different metals or differently processed metals in the same groove geometry. For the purpose of this work, a 70 nm thick layer of Al was deposited, with RMS roughness of ~1.2 nm (as verified by atomic force microscopy). Evaporation rate of Al was 1 Å/s at room temperature, at a pressure of $\sim 10^{-7}$ Torr.

First, we demonstrate experimentally light propagation within the waveguides. The experimental setup is presented in Figure 2a. Light was coupled into the waveguides by an argon-ion laser (λ_0 = 514 nm) through an inverted microscope. The polarization was controlled via a half-wave plate and a linear polarizer, placed before the microscope. The light was focused onto the sample by a 100×, 0.6 NA microscope objective having a 26.5 mm working distance. The sample was mounted on a XY micrometric translation stage (Prior Scientific Proscan II). The waveguide including both its in- and out-coupling regions were imaged by the same objective and the images were recorded by a sCMOS camera (Hamamatsu ORCA-Flash4.0 V2). Light was coupled into and out of the waveguides via the tilted nano mirrors. This solution allows the coupling of broadband radiation, in support of nonlinear and pump−probe experiments to be demonstrated in the future.

Experimental Setup and Results. Figure 2b is a schematic rendering showing the coupling scheme. Figure 2c,d shows the light coupled into and out of a L = 20 μm waveguide. The out-coupling intensity was calculated from the measurement data as a sum over the white dashed region. Background noise has been subtracted.

Qualitatively, it can be seen from the measurements that the in-coupling of a P-polarized beam (Figure 2c) resulted in weaker out-coupling as compared with the S-polarized beam (Figure 2d). This observation will be later confirmed by our simulation results (Figure 5c).

The properties of the modes supported by our V-groove aluminum plasmonic waveguide were simulated with a finite-element implementation of Maxwell's equations (COMSOL Multiphysics 4.4), while the coupling of the laser beam into and out of the waveguide was explored by a 3D simulation using a finite-difference-time-domain method (FDTD, Lumerical). Both calculations were done at the free-space wavelength of λ_0 = 514 nm. In our simulations, the optical index for Al at λ = 514 nm was taken to be $n = 0.862 + 6.225i$, based on the CRC Handbook of Chemistry and Physics.[27]

The modal simulations presented in Figure 3 show that our waveguide supports three plasmonic modes with varying degree of localization and propagation lengths. The normal amplitude of the total field is shown in red, while the direction of the field in the cross-section plane is illustrated by the arrows (of course hereby suppressing the E_z field component). Note the higher intensity scale[27] in Figure 3a for visualization clarity. The simulations show that the dominant part of the E-field is indeed perpendicular to the metal−dielectric interface, which is a generic property of plasmonic modes.[28] However, due to the nonplanar geometry of the waveguide, the modes support electric field components in all directions, and therefore, both

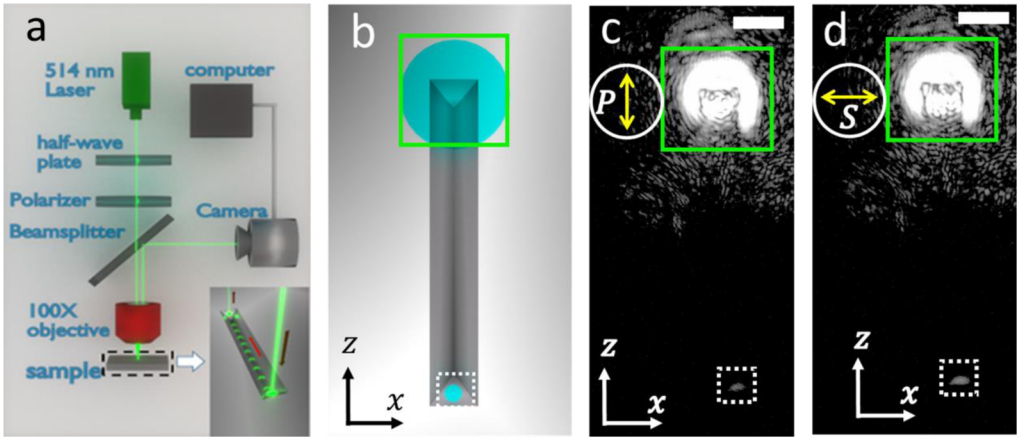

Figure 2. (a) Schematic illustration of the experimental setup. 514 nm laser is directed into microscope objective via half-wave plate and a polarizer. The beam is then coupled into the plasmonic waveguide (inset), and the out-coupling is recorded with a CMOS camera. (b) Schematic illustrations of measurements (in-coupling, green solid square; out-coupling, white dashed square). (c) Coupling measurement of waveguide with P-polarized excitation. (d) Coupling measurement of waveguide with S-polarized excitation. Polarization shown next to in-coupling spot. Scale bar 5 μm.

DOI: 10.1021/acsphotonics.6b00648
ACS Photonics 2016, 3, 2150−2157

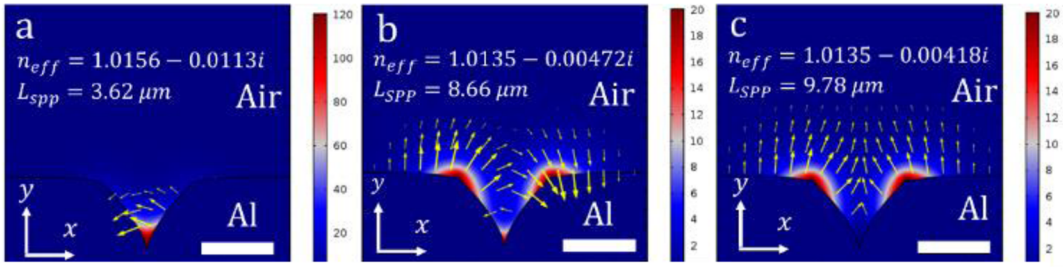

Figure 3. Simulations of the three different plasmonic modes supported by the waveguide. The normal amplitude of the total field is shown in red while the direction of the field in the cross-section plane is illustrated by the arrows. The modes vary in propagation length and field localization, from modes with high localization and short propagation length (a) to low localization and high propagation length. The modes also differ by the field components symmetry: the modes presented in (a) and (b) are symmetric in their E_x component and are antisymmetric in their E_y components, and mode (c) is antisymmetric in its E_x component and is symmetric in its E_y component. Scale bar is 2 μm.

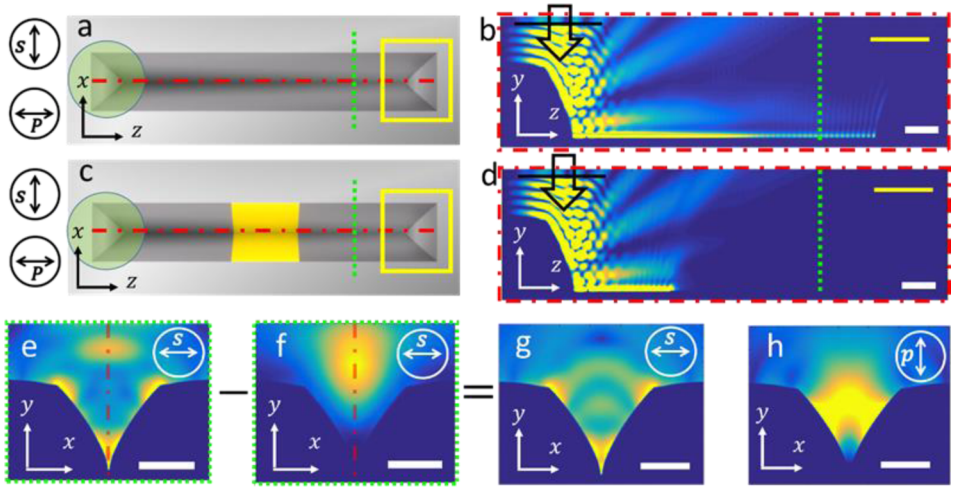

Figure 4. 3D FDTD simulations of a Gaussian beam propagation through the waveguide. (a) Schematic illustration of the waveguide, source (green circle, left end) and the different simulation detectors (solid square and dashed lines). (b) Cross-section of the simulation for S-polarized beam along the waveguide's main axis (red dashed line, a). The Gaussian source is located on the upper left corner (black line and arrow). It can be seen that, while some light reflects as free space radiation, a significant portion of it couples into plasmonic modes (yellow strip at the bottom). (c) Schematic illustration of the same waveguide with a gold patch in the center. (d) Cross-section of a simulation of the waveguide with the additional gold patch along the main axis (red dashed line, c). (e) Cross-section of the electric field along the short axis of a waveguide (green dotted line, a). (f) Cross-section of the electric field along the short axis of a waveguide with a gold patch (green dotted line, c). It can be seen that the gold patch effectively quenches the plasmonic modes and allows only the reflected beam to propagate further. (g) The result of the subtraction of the electric field of the gold-added simulation (f, only reflections) from the electric field of the unperturbed waveguide simulation (e). This is effectively the electric field of the plasmonic modes excited by the S-polarized beam (h) same as (g), for P-polarization excitation.

orthogonal polarizations of a free-space beam (perpendicular and parallel to the main axis of the waveguide, denoted S-polarization and P-polarization, respectively) can be coupled to the waveguide modes, albeit with varying coupling efficiency. In a realistic scenario, the output of the waveguide is expected to be a superposition of those modes, and thus the propagation length of optical power will be a weighted average of the propagation lengths for the individual modes, with a different weight distribution for each polarization. Measuring the output of the waveguides for each polarization provides us with a useful tool for the analysis of the relative contributions of the various modes.

We also note that such waveguides support high-order lossy modes, which are dark modes in waveguides with mirror symmetry (i.e., they are not exited in idealized simulations), while any slight asymmetry allows in-coupling of optical power that is subsequently lost. Such modes were recently unveiled by EELS.[29] It is important to notice that the modes differ in their field component symmetry: the modes presented in Figure 3a,b are symmetric in the E_x field component and are antisymmetric in the E_y field component, while the mode in Figure 3c is antisymmetric in the E_x field component and is symmetric in the E_y field component.

Literature reports that aluminum form a stable alumina layer on its surface, of about 3 nm thick, within few hours under standard laboratory conditions.[15] Modal simulations which include this additional layer show negligible effect on the spatial distribution of the modes, while the propagation lengths decrease by about 10−15%. It should be noted also that similar simulations done with Au indicate propagation lengths as short as few hundreds of nanometers. We have also simulated the propagation length of Ag-coated waveguide and found out results that are in the same order of magnitude as Al. Yet, while Al retain decent performance at shorter wavelengths, the propagation length of Ag decreases drastically with the decrease in wavelength. As discussed above, these results demonstrate the advantages of Al plasmonics toward the UV−vis regime.

Figure 4 shows the 3D FDTD simulations for the propagation of Gaussian beam arriving from free space into the nanocoupler at one end and out-coupled from the

DOI: 10.1021/acsphotonics.6b00648
ACS Photonics 2016, 3, 2150−2157

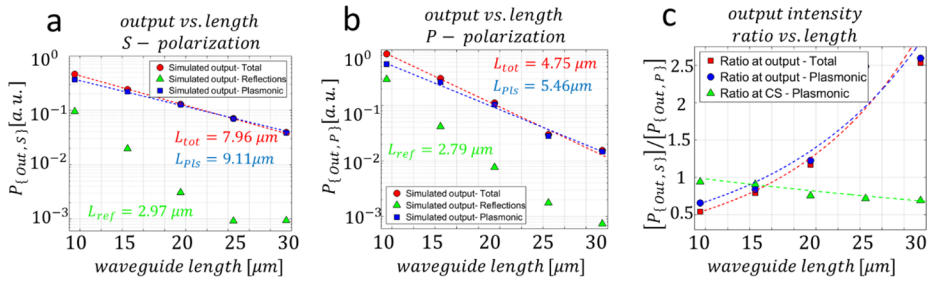

Figure 5. (a,b) Simulated waveguide output intensity as a function of waveguide length, for S-polarized and P-polarized excitation beam. Plots are presented in semilogarithmic scale, Dashed lines represent exponential fits for the data. In both polarizations we see that the reflections (green triangles) have a significant contribution to the total output (red circles) at the shorter waveguides, but for the longer waveguides, the output is solely plasmonic (blue squares). (c) Ratio between S-polarization intensity to P-polarization intensity, for the total output (red squares) and the plasmonic output (blue circles) at different lengths. Dashed lines represent the ratio between the exponential fits, as presented in figures a,b. A positive trend can be seen, which indicates that the P-polarization output decrease more rapidly with distance than the S-polarization, which is also indicated by the smaller propagation length. The ratio of intensities for the cross-section (Figure 4g,h) is represented by green triangles and shows a decreasing trend.

waveguide at the other end. The simulations were performed on five waveguides with a length varying from 10 to 30 μm with either S- or P-polarization (total of 10 simulations). The electric field components were recorded by different simulation detectors (see Figure 4a for schematic illustration of the source and monitors along the waveguide). Figure 4b shows a cross-section along the waveguide's long axis of the electric field intensity ($|E|^2$) for S-polarization excitation (coming from the upper right corner, black arrow). It can be seen that a significant portion of the excitation beam couple into plasmon-polaritons and propagate along the waveguide. The plasmonic attenuation due to Ohmic loss is also visible. It is also apparent that a portion of the free space beam does not couple into plasmons, but instead reflects from the nanocoupler as free space radiation. (A short video, demonstrating coupling, propagation and reflection, can be found in the Supporting Information.)

In order to separate the effects of reflections from the guided modes in the simulations, a second set of simulations were performed, with a 5 μm fictitious section of gold in the center of the waveguides (see Figure 4c). As mentioned above, Ohmic losses of gold are very high in the short wavelength part of the visible regime, primarily due to interband transitions. According to waveguide simulations, the propagation lengths of plasmonic modes in the gold segments are between 380 to 53 nm (at the free space wavelength of λ = 514 nm). Therefore, while the gold section does not affect the in-coupling into plasmonic modes and reflections, it effectively quenches the plasmonic propagation, and leaves only the reflected light (Figure 4d).

Figure 4e,f shows the electric field intensity recorded at a monitor along the short axis of a 10 μm waveguide, placed beyond the middle section (green dashed line, Figure 4a,b), for the regular simulation (Figure 4e) and the gold-added simulation (Figure 4f), both excited with S-polarization. Subtracting the field in Figure 4f from the field in Figure 4e yields the field distribution of the excited plasmonic modes propagating in the waveguide. The results of this procedure are presented in Figure 4g ($E_{pls} = E_{tot} - E_{ref}$). Figure 4h present the result of the same process for a P-polarization.

We assessed the output from the waveguide as a function of waveguide length and polarization by placing a simulation detector above the second nanocoupler to measure the out-coupling. In order to differentiate between out-coupling from the second nanocoupler and reflections from the first nanocoupler, we have propagated the electric field measured in the simulation detector to a far-field half-sphere and integrated only the light that propagated perpendicularly to the detector plane. As before, the simulations were performed for both S- and P-polarization with and without a gold patch. Figure 5a,b show the out-coupling intensity versus the different lengths for S- and P-polarizations, respectively, for the total out-coupling (red circles), only reflections (green triangles), and only plasmonic modes (blue rectangles).

The theoretical output-to-input ratio of the optical power for a plasmonic waveguide can be fitted as $P_{out}/P_{in} = Ae^{-(z/L)}$, where L corresponds to the effective propagation length of the signal and A corresponds to the coupling efficiency. An exponential fit was applied to the measurements. It should be mentioned that the attenuation of the reflected beam does not purely follows an exponential decay low but were, nevertheless, fitted with an exponential fit for sake of comparison. In both polarizations, reflections (simulation data indicated by green triangles) contribute a significant portion of the total out-coupling (red circles) signal in the shorter waveguides, especially in the P-polarization. The contribution of reflections decreases significantly in the longer waveguides (from 35% of the output to 5% for the P-polarization and from 20% to 2.5% in S-polarization). The subtraction of reflections is thus important for revealing the propagation length of the plasmonic modes. Indeed, doing so for both polarizations yields an effective propagation length for the plasmonic signal that exceeds the propagation length of the total signal by 15%.

Figure 5c shows the ratio between the different polarizations out-coupling ($R = [P_{\{out,S\}}]/[P_{\{out,P\}}]$ for the different waveguide lengths, with and without reflection subtraction (blue squares and red circles, respectively). The ratio has a clear positive trend, which corresponds to the observation that the effective propagation length of the plasmonic modes of S-polarization (9.11 μm) is significantly larger than the effective propagation length of the plasmonic modes of P-polarization (5.46 μm). The simulated propagation lengths are detailed in Table 1. It is interesting to note the reflected beam decays faster than the plasmonic mode. This is because this beam is propagating at a relatively large angle with respect to the main axis and thus its overlap with the output coupling region vanishes already at short propagation distances.

To further characterize the propagating signal, we calculated the overlap integral between the plasmonic electric field recorded at the short cross-section for different lengths (Figure 6a) and the mode profiles from our waveguide simulations

DOI: 10.1021/acsphotonics.6b00648
ACS Photonics 2016, 3, 2150−2157

Table 1. Simulated Propagation Lengths for S- and P-Polarization

	total propagation length (μm)	plasmonic propagation length (μm)	reflection propagation length (μm)
S-polarization	7.96	9.11	2.97
P-polarization	4.75	5.46	2.79

(Figure 3) for both polarizations. The overlap was calculated using the standard formula

$$\eta_{i,j} = \frac{|\int\int \vec{E}_i(x,y)\cdot\vec{E}_j(x,y) \times \mathrm{d}x\mathrm{d}y|^2}{\int\int|\vec{E}_i(x,y)|^2\mathrm{d}x\mathrm{d}y\cdot\int\int|\vec{E}_j(x,y)|^2\mathrm{d}x\mathrm{d}y}$$

Here, E_i is the field excited in the waveguide by either S- or P-polarization and E_j is the electrical field of modes as presented in Figure 3. The results of the calculation are presented in Figure 6c,d, and represent the effective contribution of each mode to the general field propagating in the waveguide at the recorded distance. As can be expected, the S-polarization, which is symmetrical along the x-axis, excited only the modes with a symmetrical E_x component (Figure 3a,b), while the P-polarization, which is symmetrical along the y-axis, excites the E_y-symmetrical mode (Figure 3c).

It can be observed in Figure 6c that the contribution of the first mode (Figure 3a) to the S-polarized propagation decreases with distance, which can be attributed to its relatively short propagation length (3.62 μm). However, the contributions of the second and third modes (Figure 3b,c) increase significantly with length. This can be understood when considering that not all of the surface plasmons polaritons excited by the free space beam couple into guided modes of the waveguide, while instead propagating as more common surface modes, as will be discussed shortly.

Figure 6b shows the electric field intensity at the surface level of a 15 μm long waveguide excited with P-polarization. Monitor location is depicted in the second image on the bottom row of Figure 6a (red dashed line). The outline of the waveguide is imposed on the image (black dashed line). Due to the location of the detector, the guided modes are not visible, but we can see that there are surface modes that propagate at an angle to the waveguide's long axis. Similar to the effect of reflections, the surface modes contributes to the total intensity of the electric field in the shorter waveguides, but this contribution decreases in the longer waveguide (due to the angle of propagation), which leads to the increase in the guided modes' contribution to the overall energy, as presented in Figure 6c,d.

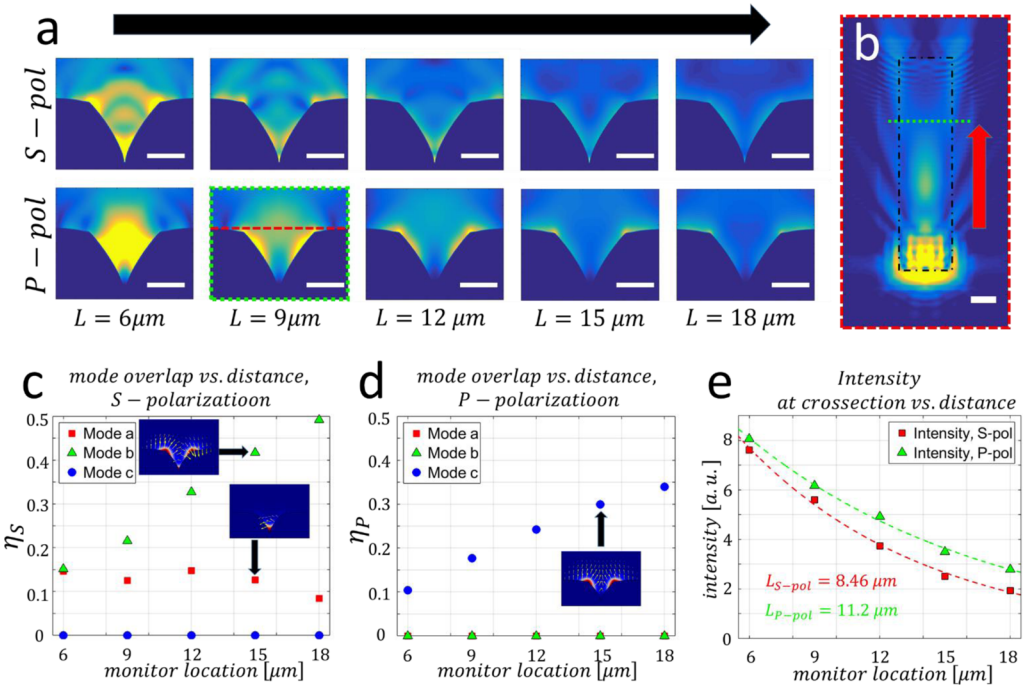

Figure 6. Analysis of the waveguide cross-section simulation monitor. (a) Electric field distribution in waveguides excited by S-polarized beam (top row) and P-polarized beam (bottom row). It can be seen that the S-polarization excitation couples into modes that are confined to the apex and the shoulders of the waveguide, while the P-polarization excitation couples into modes that are confined only to the shoulders of the waveguide, with no field at the apex. Scale bar is 2 μm. (b) Top view of the electric field at surface level of a 15 μm waveguide excited by P-polarized beam (detector location indicated in (a), bottom row, second image, red dashed line). As can be seen, some of the light couples into surface modes that propagate at an angle to the waveguide's main axis. For small angles, these nonguided modes pass around the second nanocoupler and continue beyond it. Scale bar is 2 μm. (c, d) Calculation of modal overlap with the simulated S-polarized and P-polarized excitations, for the modes presented in Figure 3. Modes that have a symmetric E_x component and an antisymmetric E_y component were excited solely by the S-polarized beam (c), while the mode with symmetric E_y component and an antisymmetric E_x component was excited solely by the P-polarized beam. The increase in overlap with distance for modes b,c is likely due to the leakage of the nonguided modes. (e) Simulated intensities at the cross-section detector for S-polarization (red circles) and P-polarization (green triangles). It can be seen that at the cross-section, plasmonic modes excited by P-polarization have a longer propagation length. However, this intensity calculation includes surface modes which do not couple well out of the second nanocoupler and, therefore, contribute less power to the total output in longer waveguides.

DOI: 10.1021/acsphotonics.6b00648
ACS Photonics 2016, 3, 2150−2157

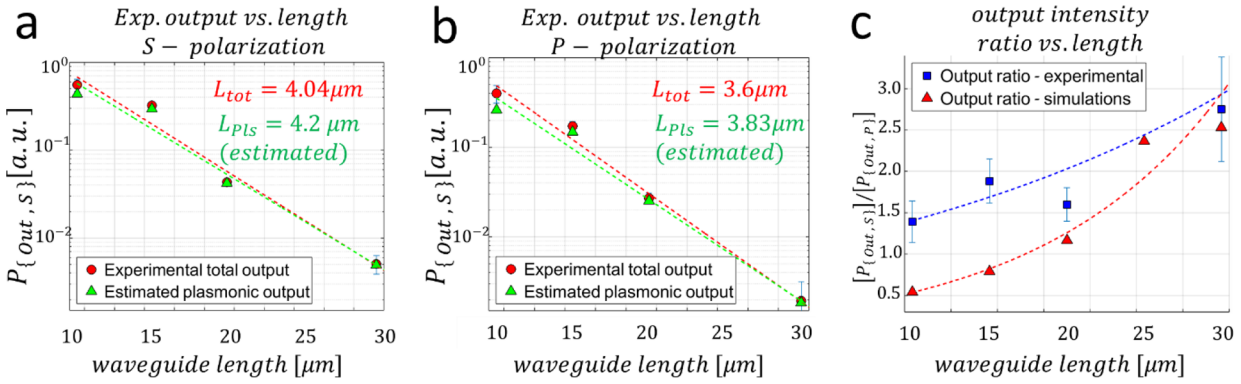

Figure 7. (a, b) Experimental output intensity from the waveguide as a function of waveguide length, for S-polarized and P-polarized excitation beam (red circles). Using the data from the gold-added simulation (Figure 4a,b), we extract the estimated plasmonic contribution to output intensity (green triangles). Plots are presented in semilogarithmic scale; dashed lines represent the linear fit for the data. (c) Experimental output intensity ratio (blue squares) alongside with the calculated value (red triangles, extracted from Figure 5c) and experimental measurements (blue squares). Dashed lines represent the ratio between the exponential fits, as presented in Figure 4a,b and (a) and (b) of this figure. It can be seen that both ratios present a positive trend.

The effects of the surface modes also explain the positive trend in ratios presented in Figure 5c. When considering Ohmic loss alone, the propagation length of the P-polarized/E_y symmetric mode is relatively higher than that of the S-polarized/E_x symmetric modes, which should yield a negative trend in ratios (i.e., a stronger output for the P-polarization with distance, in relation to the S-polarization). We calculated the total intensity of the plasmonic fields at the cross-section of the waveguide and nearby surfaces for both polarizations (Figure 6e). From these calculations, we extracted the ratio between those intensities (Figure 5c, green triangles). The calculations indeed yield a longer propagation length of plasmons excited by P-polarization (11.2 μm) than that of S-polarized plasmons (8.46 μm), and thus, the ratio shows a negative trend.

However, as was demonstrated in previous works,[17] in such V-groove-based plasmonic waveguides, more light couples into plasmonic waveguide modes under S-polarized excitation rather than under P-polarized excitation. This is because more S-polarized modes are available and the overlap between the excitation beam and those modes is higher. It can be seen in Figure 5c,d that the total contribution of the E_x-symmetrical modes is 29.8% of the total energy, while the contribution of the E_y-symmetrical mode is only 10.3%. Other simulations (not included) showed that the contribution of E_x-symmetrical modes is about 6.5× higher than that of the E_y-symmetrical modes. Light that does not couple to waveguide modes is either reflected back into free space or couples forward into nonguided modes. As explained above, the contribution of the nonguided modes to the output decreases rapidly with propagation distance. Thus, while in the shorter waveguides the output of the P-polarized simulation is stronger, at the longer waveguides the output of the waveguide is stronger for S-polarization, since it couples mostly more efficiently to the guided modes.

Following the elaborated study of the modal properties, we can now measure their properties and analyze the data based on the simulation results. Indeed, we have coupled light to several waveguides, with lengths ranging between 10 and 30 μm, for both S- and P-polarizations, and measured the output signal. Figure 7a,b shows the measured out-coupling intensity versus the different lengths for S- and P-polarization, respectively (red circles). In light of the simulations, we assume that the total output signal consists of both plasmonic modes and reflections with the weight of each varying with the waveguide's length. We calculated the plasmonic fraction (PF) for each length according to simulations $\mathrm{PF}(l) = 1 - \frac{[\text{reflections output intensity}(l)]}{[\text{total output intensity}(l)]}$. We then multiply the plasmonic fraction with the total experimental output to get the estimated plasmonic output, shown in Figure 7a,b (blue squares). An exponential fit was applied for both measurements, yielding propagation lengths, as detailed in Table 2.

Table 2. Experimentally Measured Propagation Lengths for S- and P-Polarization

	total propagation length (μm)	plasmonic propagation length (μm; estimated)
S-polarization	4.02	4.2
P-polarization	3.6	3.83

Figure 7c presents the ratio between the out-coupling of both polarizations (blue squares). Indeed, we observe a similar trend as in the simulations (red triangles). Moreover, the S-polarization also resulted in a longer propagation length than P-polarization, also in agreement with the simulation results (Table 2). The experimental propagation length is shorter than that of the simulated propagation length in both polarizations. This can be attributed to local scattering inside the waveguide caused by surface roughness, and also by the additional 3 nm alumina layer, that is expected to decrease the propagation length, as discuss before.

DISCUSSION

We have demonstrated the viability of the aluminum V-groove waveguide as a plasmonic waveguide for visible light. While it is excitable from both S- and P-polarization, it was shown that it is preferable to excite it with S-polarization in order to achieve higher output and longer propagation length. Much improvement can be achieved by optimizing the fabrication process, that is, adjusting the geometry of the V-groove curve by adjusting the time of exposure to the thermal oxidation fabrication step[17] (Figure 1d). This would enable us to tailor the waveguide characteristics even further, for example, to

DOI: 10.1021/acsphotonics.6b00648
ACS Photonics 2016, 3, 2150−2157

create a single mode waveguide, achieve higher localization, or increase the propagation length and decrease the radiation loss of modes. Different waveguide characteristics could be of interest for different applications. A single mode waveguide with higher confinement may be used for light−matter interactions such as applications with coupling to single quantum emitters[22] and even for creating single-photon transistors.[30] Moreover, many biomolecules contain intrinsic fluorophores that naturally fluoresce in the short visible and near UV, and the ability of the V-groove waveguide to nanofocus electromagnetic energy[20] could offer a way to probe such molecules, label-free, and it was already shown that aluminum nanostructured films were able to enhance fluorescence of biomolecules in the near UV regime.[31] Extended propagation lengths in the short-visible regime can allow us to integrate V-groove waveguides in optical devices such as a near-field optical magnifier (NFOM)[10] or use it for lab-on-chip biosensing applications. Many biolabels, such as Green Fluorescent Protein, emit at the short visible regime and are already being used for bacterial biosensing of chemical hazards.[32]

A plasmonic nanowaveguide could be vital in connecting a bacterial biosensor with an on-chip detector.

One should note that while the current experimental work was based on an Ar-ion laser line at 514 nm wavelength, these waveguides are even more appealing for applications at shorter wavelengths, where Au and even Ag layers cannot be used. We intend to demonstrate the operation at shorter wavelengths in the near future.

Finally, it should be noted that our Al-coated waveguides show similar behavior over the course of few weeks of measurements. This is attributed to the formation of a stable alumina layer which protects the Al from further oxidation and deterioration. This serves as another indication for the attractiveness of Al coated plasmonic waveguides as a robust solution for the UV and the short visible regime.

■ ASSOCIATED CONTENT

Supporting Information

The Supporting Information is available free of charge on the ACS Publications website at DOI: 10.1021/acsphotonics.6b00648.

Supporting movie (AVI).

■ AUTHOR INFORMATION

Corresponding Author

*E-mail: ulevy@mail.huji.ac.il.

Notes

The authors declare no competing financial interest.

■ ACKNOWLEDGMENTS

We acknowledge financial support from the Danish international network Program (Grant No. 1370-00124B) with Israel.

■ REFERENCES

(1) Sorger, V. J.; Oulton, R. F.; Ma, R.-M.; Zhang, X. Toward Integrated Plasmonic Circuits. *MRS Bull.* **2012**, *37*, 728−738.

(2) Fang, Y.; Sun, M. Nanoplasmonic Waveguides: Towards Applications in Integrated Nanophotonic Circuits. *Light: Sci. Appl.* **2015**, *4*, e294.

(3) Gramotnev, D. K.; Bozhevolnyi, S. I. Plasmonics beyond the Diffraction Limit. *Nat. Photonics* **2010**, *4*, 83−91.

(4) Ebbesen, T. W.; Genet, C.; Bozhevolnyi, S. I. Surface-Plasmon Circuitry. *Phys. Today* **2008**, *61*, 44−50.

(5) Arbel, D.; Orenstein, M. Plasmonic Modes in W-Shaped Metal-Coated Silicon Grooves. *Opt. Express* **2008**, *16*, 3114.

(6) Berini, P. Figures of Merit for Surface Plasmon Waveguides. *Opt. Express* **2006**, *14*, 13030.

(7) Babicheva, V. E.; Shalaginov, M. Y.; Ishii, S.; Boltasseva, A.; Kildishev, A. V. Long-Range Plasmonic Waveguides with Hyperbolic Cladding. *Opt. Express* **2015**, *23*, 31109.

(8) Johnson, P. B.; Christy, R. W. Optical Constants of the Noble Metals. *Phys. Rev. B* **1972**, *6*, 4370−4379.

(9) Estevez, M. c.; Alvarez, M.; Lechuga, L. m. Integrated Optical Devices for Lab-on-a-Chip Biosensing Applications. *Laser Photonics Rev.* **2012**, *6*, 463−487.

(10) Rose, A. H.; Wirth, B. M.; Hatem, R. E.; Ahmed, A. P. R.; Burns, M. J.; Naughton, M. J.; Kempa, K. Nanoscope Based on Nanowaveguides. *Opt. Express* **2014**, *22*, 5228.

(11) Mao, J.; Blair, S. Nanofocusing of UV Light in Aluminum V-Grooves. *J. Phys. D: Appl. Phys.* **2015**, *48*, 184008.

(12) Knight, M. W.; King, N. S.; Liu, L.; Everitt, H. O.; Nordlander, P.; Halas, N. J. Aluminum for Plasmonics. *ACS Nano* **2014**, *8*, 834−840.

(13) Swartz, M.; Rodriguez, M.; Quast, A. D.; Cooper, C. T.; Blair, S.; Shumaker-Parry, J. S. Aluminum Nanocrescent Plasmonic Antennas Fabricated by Copper Mask Nanosphere Template Lithography. *J. Phys. Chem. C* **2016**.*120*2059710.1021/acs.jpcc.6b00396

(14) Cheng, L.; Huang, L.; Li, X.; Wu, J.; Zhang, Y.; Wang, J.; Cheng, L.; Liu, Y.; Feng, X.; Zhang, W.; Cai, Y. UV Plasmonic Resonance of Aluminum Shallow Pit Arrays. *J. Phys. Chem. C* **2015**, *119*, 14304−14311.

(15) Langhammer, C.; Schwind, M.; Kasemo, B.; Zorić, I. Localized Surface Plasmon Resonances in Aluminum Nanodisks. *Nano Lett.* **2008**, *8*, 1461−1471.

(16) Gérard, D.; Gray, S. K. Aluminium Plasmonics. *J. Phys. D: Appl. Phys.* **2015**, *48*, 184001.

(17) Smith, C. L. C.; Thilsted, A. H.; Garcia-Ortiz, C. E.; Radko, I. P.; Marie, R.; Jeppesen, C.; Vannahme, C.; Bozhevolnyi, S. I.; Kristensen, A. Efficient Excitation of Channel Plasmons in Tailored, UV-Lithography-Defined V-Grooves. *Nano Lett.* **2014**, *14*, 1659−1664.

(18) Fernandez-Cuesta, I.; Nielsen, R. B.; Boltasseva, A.; Borrisé, X.; Pérez-Murano, F.; Kristensen, A. V-Groove Plasmonic Waveguides Fabricated by Nanoimprint Lithography. *J. Vac. Sci. Technol. B* **2007**, *25*, 2649−2653.

(19) Nielsen, R. B.; Fernandez-Cuesta, I.; Boltasseva, A.; Volkov, V. S.; Bozhevolnyi, S. I.; Klukowska, A.; Kristensen, A. Channel Plasmon Polariton Propagation in Nanoimprinted V-Groove Waveguides. *Opt. Lett.* **2008**, *33*, 2800.

(20) Volkov, V. S.; Bozhevolnyi, S. I.; Rodrigo, S. G.; Martín-Moreno, L.; García-Vidal, F. J.; Devaux, E.; Ebbesen, T. W. Nanofocusing with Channel Plasmon Polaritons. *Nano Lett.* **2009**, *9*, 1278−1282.

(21) Kumar, S.; Lausen, J. L.; Garcia-Ortiz, C. E.; Andersen, S. K. H.; Roberts, A. S.; Radko, I. P.; Smith, C. L. C.; Kristensen, A.; Bozhevolnyi, S. I. Excitation of Surface Plasmon Polariton Modes with Multiple Nitrogen Vacancy Centers in Single Nanodiamonds. *J. Opt.* **2016**, *18*, 24002.

(22) Bermúdez-Ureña, E.; Gonzalez-Ballestero, C.; Geiselmann, M.; Marty, R.; Radko, I. P.; Holmgaard, T.; Alaverdyan, Y.; Moreno, E.; García-Vidal, F. J.; Bozhevolnyi, S. I.; Quidant, R. Coupling of Individual Quantum Emitters to Channel Plasmons. *Nat. Commun.* **2015**, *6*, 7883.

(23) Bozhevolnyi, S. I.; Volkov, V. S.; Devaux, E.; Laluet, J.-Y.; Ebbesen, T. W. Channel Plasmon Subwavelength Waveguide Components Including Interferometers and Ring Resonators. *Nature* **2006**, *440*, 508−511.

(24) Burgos, S. P.; Lee, H. W.; Feigenbaum, E.; Briggs, R. M.; Atwater, H. A. Synthesis and Characterization of Plasmonic Resonant Guided Wave Networks. *Nano Lett.* **2014**, *14*, 3284−3292.

DOI: 10.1021/acsphotonics.6b00648
ACS Photonics 2016, 3, 2150−2157

(25) Smith, C. L. C.; Desiatov, B.; Goykmann, I.; Fernandez-Cuesta, I.; Levy, U.; Kristensen, A. Plasmonic V-Groove Waveguides with Bragg Grating Filters via Nanoimprint Lithography. *Opt. Express* **2012**, *20*, 5696.
(26) Smith, C. L.; Stenger, N.; Kristensen, A.; Mortensen, N. A.; Bozhevolnyi, S. I. Gap and Channeled Plasmons in Tapered Grooves: A Review. *Nanoscale* **2015**, *7*, 9355−9386.
(27) Hdbk Chemistry and Physics, http://hbcponline.com/faces/documents/12_23/12_23_0002.xhtml (accessed Oct 4, 2016).
(28) Maier, S. A. *Plasmonics: Fundamentals and Applications*; Springer, 2007.
(29) Raza, S.; Stenger, N.; Pors, A.; Holmgaard, T.; Kadkhodazadeh, S.; Wagner, J. B.; Pedersen, K.; Wubs, M.; Bozhevolnyi, S. I.; Mortensen, N. A. Extremely Confined Gap Surface-Plasmon Modes Excited by Electrons. *Nat. Commun.* **2014**, *5*, 4125.
(30) Chang, D. E.; Sørensen, A. S.; Demler, E. A.; Lukin, M. D. A Single-Photon Transistor Using Nanoscale Surface Plasmons. *Nat. Phys.* **2007**, *3*, 807−812.
(31) Ray, K.; Chowdhury, M. H.; Lakowicz, J. R. Aluminum Nanostructured Films as Substrates for Enhanced Fluorescence in the Ultraviolet-Blue Spectral Region. *Anal. Chem.* **2007**, *79*, 6480−6487.
(32) Elad, T.; Almog, R.; Yagur-Kroll, S.; Levkov, K.; Melamed, S.; Shacham-Diamand, Y.; Belkin, S. Online Monitoring of Water Toxicity by Use of Bioluminescent Reporter Bacterial Biochips. *Environ. Sci. Technol.* **2011**, *45*, 8536−8544.

DOI: 10.1021/acsphotonics.6b00648
ACS Photonics 2016, 3, 2150−2157